Role of Hydrogen Bonds in Controlling the Morphology of Self-Assembling Carbamate Systems

Mohammad Moniruzzaman and Pudupadi R. Sundararajan*

Department of Chemistry, Carleton University, 1125 Colonel By Drive, Ottawa, Ontario K1S 5B6, Canada

Received: September 28, 2004; In Final Form: November 9, 2004

With a view to understand the role of hydrogen bonding in controlling the morphology of self-assembling carbamate systems, *N*-octadecylcarbamate dodecyl ester was blended individually with a low molecular weight polyethylene and two commercial clarifiers, namely Kemamide S and Kemamide E 180. The effect of blending on the morphology of this long chain carbamate was investigated using optical microscopy, differential scanning calorimetry, and X-ray diffraction. The crystal structure of the carbamate was not affected by the addition of polyethylene or Kemamide S. The heterogeneous nucleation of the carbamate by the polyethylene or Kemamide S resulted in the reduction of the spherulite size of the carbamate, but it did not improve the transparency of the sample due to phase separation. On the other hand, significant improvement of transparency was achieved when the carbamate was blended with Kemamide E 180. Blending reduced the crystallite and spherulite size, heat of fusion, and crystallinity. An exchange of hydrogen bonds between the carbamate and Kemamide E is indicated in the IR spectra, and this affects the packing of the alkyl chains of the carbamates. This heterogeneous blending shows similar effects on the morphology as was achieved by blending two homologous carbamates in our previous study (*J. Phys. Chem. B* **2003**, *107*, 8416).

Introduction

Understanding of the mechanism of self-assembly facilitated by hydrogen bonds, π-stacking, charge-transfer complex, etc. is key to the sophisticated use of such self-assembling materials, which include liquid crystals, block copolymers, hydrogen and π-bonded complexes, and many natural polymers. The wisdom to control these drivers of self-assembly is essential for the development of new materials for advanced technologies. Carbamates are an important class of self-assembling materials that have found numerous applications, such as for increasing the abrasion resistance of polyurethane compositions[1], improving the hardness of urethane-based adhesives and sealants[2], adjusting the viscosity value of oils and greases, and as insecticides.[3,4] Due to the semicrystalline nature and low melt viscosity (∼10 cP), carbamates with alkyl side chains have potential applications as vehicles in reprography and ink jet printing technologies.[5−8] Since these materials form spherulites when solidified, controlling the size of the spherulites is important. Large spherulites would lead to brittle, opaque, and hazy prints. Ideally, the spherulite size should be on the order of the wavelength of visible light.

In a previous paper,[9] we reported the synthesis, morphology, and thermal behavior of some long-chain monocarbamates having 22−36 carbon atoms in the alkyl side chain. With a view to control the crystalline morphology of these carbamates, we blended two homologous carbamates at different compositions. It was found that blending of two homologous carbamates is an efficient way to reduce the crystal/spherulite size and crystallinity of these self-assembling compounds. A significant improvement of transparency of the sample was achieved with the blending. These results prompted us to further our study on the changes in morphology of the blends of a carbamate with stearic acid,[10] which is another hydrogen-bonded system that has some structural similarities with the carbamate. However, stearic acid was less effective in controlling the morphology and transparency of the carbamate as compared to the blends of two homologous carbamates. On the other hand, when the carbamate was the minor component in the blend, there was a reduction of crystal size of stearic acid and improvement of its transparency as compared to those of pure stearic acid. The powder X-ray diffractograms of the blends showed a significant decrease in the intensity of the long spacing (d = 40 Å) of stearic acid, indicating that the presence of carbamate as a minor component in the blends might result in the disruption of the crystal lattice of stearic acid to some extent. The results of these studies raised the question as to the underlying factor that plays a role in the reduction of spherulite size and crystallinity and the improvement of transparency.

The FTIR spectra of the carbamates indicated that all the C═O and N−H groups are hydrogen bonded. In the case of the blends of homologous carbamates, the IR spectra did not show any change in the intensity or position of the C═O and NH stretching frequency of the carbamates as compared to that of the pure components. This led us to conclude that the extent of hydrogen bonding was not affected by blending and that the changes in morphology were due to the disrupted packing of the alkyl chains in the blends. The IR spectra of the carbamate/stearic acid blends showed only one C═O stretch, which indicated the possibility that an interaction between the components in the blends had affected the type of hydrogen bonding of the system. However, no definite conclusion could be made from that observation, since the C═O band of the carbamate was so close to that of stearic acid that even a physical mixing could lead to an apparently single band due to superposition. Some of the questions that arise from the above studies are (i) if the changes in morphology in the blends are due to the poor packing of the alkyl chains, what is the cause of such packing?

* Corresponding author. E-mail: Sundar@carleton.ca.

10.1021/jp045592c CCC: $30.25 © 2005 American Chemical Society
Published on Web 12/30/2004

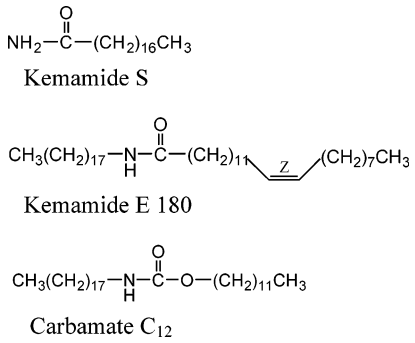

Figure 1. Structures of KemS, KemE, and C_{12}.

Is the H-bond responsible to some extent? (ii) Would a similar morphology result if this hydrogen-bonded system were blended with a non-hydrogen bonded system having similar alkyl chains? (iii) How is the blending of homologous carbamates comparable to the use of commercial clarifiers in controlling the morphology? This paper is an attempt to address these questions.

The carbamate used for this study was *N*-octadecylcarbamate dodecyl ester. This was blended with (i) a low molecular weight polyethylene, which is a non-hydrogen-bonded system having alkyl chains similar to the carbamate, and (ii) two commercial clarifiers, Kemamide S and Kemamide E 180. These two clarifiers have similarities with the carbamate: they have long alkyl chains and they are capable of forming intermolecular hydrogen bonds. These clarifiers have been used in the patent literature.[7,8] Figure 1 shows the molecular structure of the Kemamide S, Kemamide E 180, and the carbamate C_{12}. For convenience, the carbamate, polyethylene, Kemamide S, and Kemamide E 180 will be referred to as C_{12}, PE, KemS, and KemE, respectively, throughout this paper.

For industrial applications, commercial clarifiers are usually added in a small amount (<10 wt %) to control the morphology. Higher concentration would lead to phase separation as well as an increase in the melt viscosity of the system (and hence require higher process temperatures). Therefore, concentrations of less than 25% of the clarifiers or polyethylene were used to prepare the blends with the carbamate.

Experimental Section

The synthesis and purification procedure for the carbamate were described before.[9] Polyethylene of molecular weight 655 (Petrolite Corp., courtesy of Xerox research Centre of Canada) was used. The DSC thermogram indicated a broad molecular weight distribution in the sample. Hence, it was partially dissolved in hot toluene at 80 °C, filtered at that temperature, and washed with hot toluene. The sample was dried under vacuum at 50 °C for 2 days. The dried sample showed a sharper and narrower peak in DSC, indicating a narrower molecular weight distribution. The same differences in the DSC traces were seen when the original and the hot-filtered samples were crystallized from the melt under identical conditions. This rules out the possibility that such differences could be due to the differences in the crystallinity or crystallite size between the two samples. The clarifiers Kemamide S and Kemamide E180 were purchased from Crompton Corp.

Preparation of the Blends. Binary blends of C_{12}/PE, C_{12}/KemS, and C_{12}/KemE were prepared by melt mixing, with 98/02, 95/05, 90/10, 85/15, and 80/20 (wt %) compositions. For C_{12}/KemE blends, a few more blend compositions were prepared (60/40, 50/50, 40/60, 20/80) to study the shifts of carbonyl stretching frequency in IR. Preweighed mixtures of C_{12} and PE, KemS, or KemE were heated in a 10 mL beaker at 110 °C with continuous stirring. After 1 h, the melt was slowly cooled to room temperature.

Methods for Structure and Morphology. Thermal analysis was performed using a DuPont 910 differential scanning calorimeter at a heating rate of 10 °C/min. The instrument was calibrated for temperature and energy with indium and tin reference samples. DSC traces were recorded with about 7−10 mg of sample, in a nitrogen atmosphere.

X-ray diffraction data were collected within the range $2° \leq 2\theta \leq 50°$ using a Philips automated powder diffractometer (model PW 1710) and nickel-filtered Cu Kα radiation ($\lambda = 1.542$ Å). The possible presence of texture was checked by taking additional diffractograms with samples turned in the plane of measurement by 90°. The MDI Datascan 3.2 software (Materials Data Inc., Livermore, CA) was used for data collection. The results were analyzed using MDI Jade 5.0 XRD Pattern Processing software.

The crystallite size, L corresponding to a particular X-ray reflection was calculated by the Scherrer equation:[11]

$$L = K\lambda/b \cos\theta \tag{1}$$

where λ is wavelength of the X-ray, θ is half the scattering angle, and b is the half-width of the peak on the 2θ scale in radians; $K = 0.9$.

Small angle light scattering (SALS) was used primarily in the H_v mode to detect the spherulitic crystalline morphology. The experimental setup and calculation have been described before.[12,13] Optical micrographs were recorded using a Zeiss Axioplan polarized optical microscope (OM), equipped with a Linkam hot stage. Northern Eclipse (version 6.0) image processing software was used to capture the images as well as to calculate the spherulite/crystal size. The samples for optical microscopy were prepared by melting a small amount of the material on the microscope slide at a temperature 20 °C higher than its melting point, holding it isothermally for 10 min to remove any morphological history, and then cooling it down slowly to room temperature at the rate of 10 °C/min. Another set of samples was prepared following the same procedure, but in this case the samples were quenched from the melt, instead of slow cooling.

FTIR spectroscopic measurements were carried out at ambient conditions using a Michelson M129 BOMEM Fourier Transform Infrared (FTIR) spectrometer. The data were collected using BOMEM GRAMS/386 software for later evaluation. The FTIR spectra of the samples were taken in the form of a transparent KBr pellet. A background FTIR spectrum was taken for each experiment with the identical sample holder.

The "slow-cooled" samples were prepared by melting the sample at 110 °C, turning off the hot plate, and letting the sample cool to room temperature. The samples from the melt were quickly transferred to an aluminum plate kept at room temperature to prepare quenched samples. This simulates the deposition of a hot melt ink drop from an ink jet printer to the substrate kept at room temperature.

Results and Discussion

Figure 2 shows the optical micrographs of C_{12}, KemS, PE, and KemE. The slow-cooled sample of C_{12} shows coarse spherulites (Figure 2a) with an average size of 220 μm, and the quenched sample shows regular spherulites with a classical Maltese cross (Figure 2b), the average size being 35 μm. The slow-cooled samples of KemS show highly coarse fibrillar morphology (Figure 2c) that reduces to irregularly shaped large

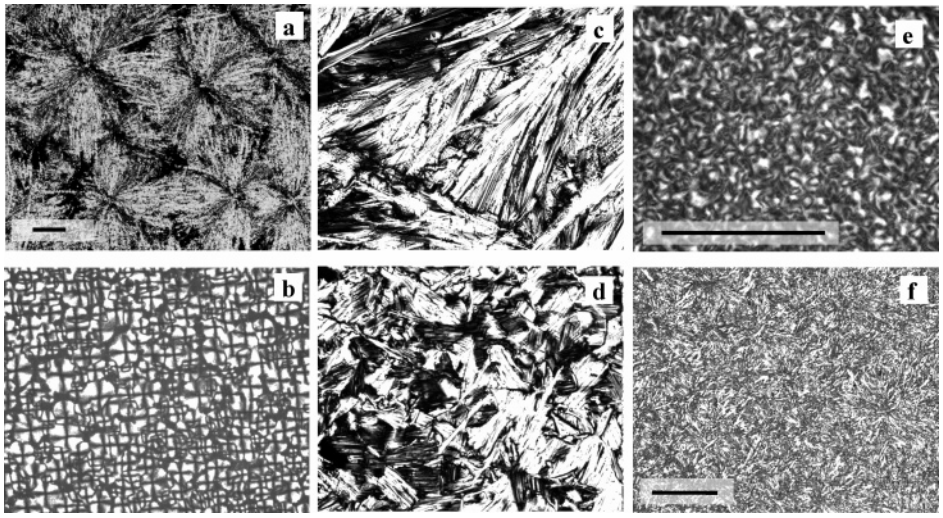

Figure 2. Optical micrographs of different samples: (a) C_{12}, slow-cooled; (b) C_{12}, quenched; (c) KemS, slow-cooled; (d) KemS, quenched; (e) PE, slow-cooled; (f) KemE, slow-cooled. Note: Scale bars represent 100 μm. The magnification is same for samples a−d.

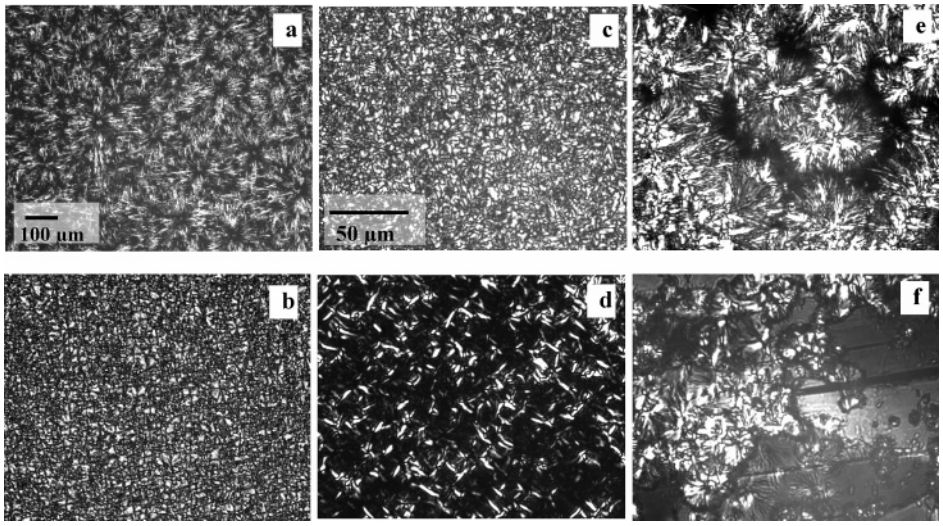

Figure 3. Optical micrographs of different blends: 90/10 blends of C_{12}/PE (a) slow-cooled and (b) quenched; 80/20 blends of C_{12}/PE (c) slow-cooled and (d) quenched; 80/20 blend of C_{12}/KemS (e and f). The magnification is same for a and b. c−f have the same magnification.

crystals in the quenched sample (Figure 2d). Parts e and f of Figure 2 show the optical micrographs of the slow-cooled samples of PE and KemE, respectively. PE shows imperfect spherulites and KemE shows fibrillar spherulites. The average size of the spherulites for the slow-cooled samples of PE and KemE were 10 and 45 μm, respectively. (The scale bar in this figure is 100 μm. The magnification is the same for all parts of Figure 2a−d). The size of the spherulites in the quenched samples of PE and KemE could not be determined.

The changes in morphology of C_{12} upon blending with PE, KemS, and KemE are discussed below.

C_{12}/PE and C_{12}/KemS Blends. The slow-cooled samples of C_{12} containing 2−5% PE show coarse spherulites with sizes that are similar to those of pure C_{12}; also in the quenched blends, the shape and size of the spherulites are similar to those of the quenched sample of pure C_{12}. As the amount of PE increases further in the blend, the size of the spherulites decreases. The optical micrographs for the slow-cooled blends of C_{12} containing 10% and 20% PE are shown in parts a and c of Figure 3, respectively, and those for the quenched blends are shown in parts b and d of Figure 3, respectively. The sizes of the spherulites in the slow-cooled blends are plotted in Figure 4 as a function of wt % of PE, which shows a decrease in the spherulite size of C_{12} with increasing concentration of PE in the blend. It is seen that with 10% PE, the spherulite size reduces from 220 to 60 μm. In the case of quenched samples, the size reduces even further, to 16 μm with 10% PE. The quenched blends containing 15 and 20% PE show only tiny crystals of ca. 6 μm size. The spherulites of C_{12}, by itself or in the blends, exhibit positive birefringence.

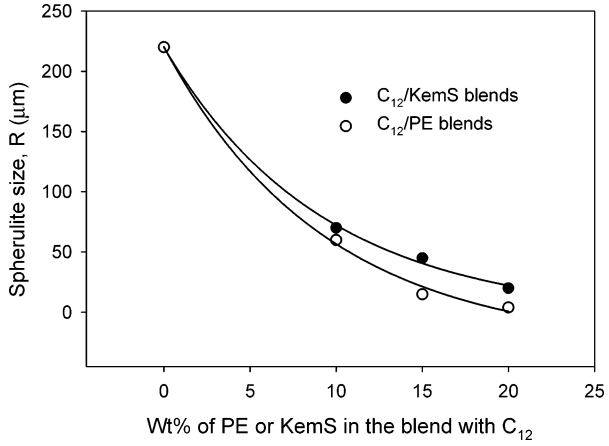

Figure 4. Spherulite size of C_{12} in the slow-cooled blend as a function of weight percent of PE or KemS.

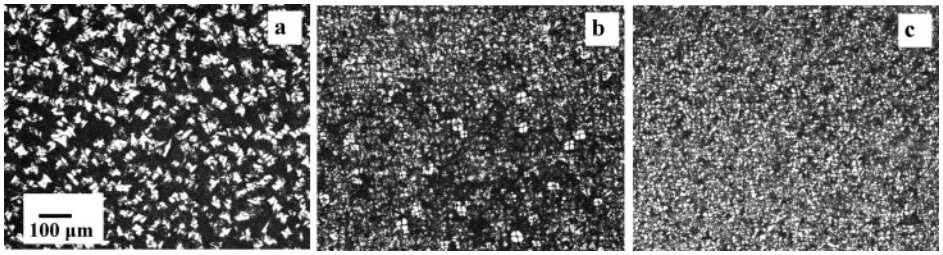

Figure 5. Optical micrographs of the slow-cooled blends of C_{12}/KemE: (a) 90/10 (b) 85/15, and (c) 80/20.

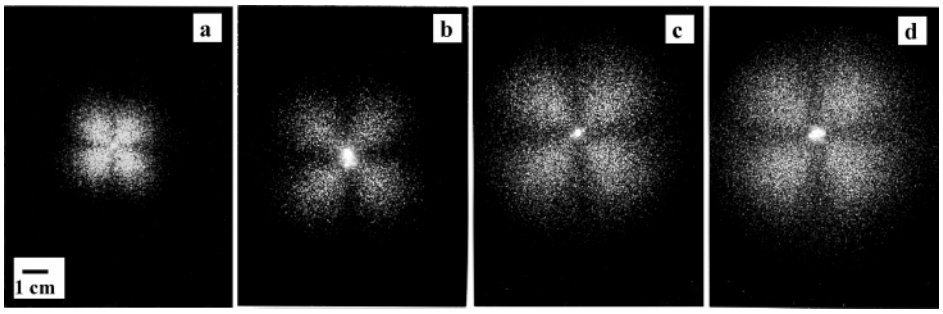

Figure 6. H_v scattering pattern for the quenched sample of (a) C_{12} and C_{12}/KemE blends at composition of (b) 98/02, (c) 90/10, and (d) 85/15.

In the slow-cooled and quenched blends of C_{12}/KemS, the spherulites of C_{12} as well as the large crystals of KemS are visible at all compositions, indicating phase separation. However, similar to C_{12}/PE blends, the spherulite size of C_{12} starts decreasing as the amount of KemS increases to 10 wt %. Figure 4 shows a gradual decrease in spherulite size with an increase in the wt % of KemS in the slow-cooled blends. In the quenched blend containing 10 wt % of KemS, the average size of the spherulites is 15 μm. The spherulites are not clearly visible in the quenched blends containing 15% and 20% KemS, but the phase-separated crystals of KemS are clearly visible.

The phase separation of C_{12} and KemS in the slow-cooled sample containing 20% KemS are shown at parts e and f of Figure 3; the micrographs were taken from the same sample, but from two different locations. It might be that a similar phase separation occurs in the C_{12}/PE blends, but the crystals of PE could not be distinguished from those of C_{12} because of their similar size in the blend. However, PE seems to be more effective in reducing the spherulite size of C_{12}, which is evident from Figure 4. For example, for the slow-cooled blends, with 20% PE, the average spherulite size is 4 μm as compared to 20 μm in the case of 20% KemS in the blend. It should be mentioned that although the addition of PE and KemS reduced the spherulite size of C_{12}, there was no significant improvement of transparency of the sample. The blending of two homologous carbamates in our previous work[9] resulted in much better transparency.

Analysis of the melting temperatures showed that the components in the C_{12}/PE and C_{12}/KemS blends exert a mutual diluent effect as seen before with the blends of the homologous carbamates.[9] With both C_{12}/PE and C_{12}/KemS blends, the X-ray diffractograms were just the superposition of those of the parent compounds, which indicates that blending with PE or KemS does not affect the crystal structure of C_{12}. This is in contrast to the case of C_{18}/stearic acid blends.[10]

In the IR spectra of C_{12}/PE blends, the positions of C═O and NH stretching bands of C_{12} (1686 and 3337 cm^{-1}, respectively) were unaffected, which indicates that PE does not disrupt the intermolecular hydrogen-bonded network of C_{12}. In fact, these bands were found to be unaffected even when C_{12} was blended with 90% PE. The C═O and NH stretching frequencies of Kemamide S are 1646 and 3394 cm^{-1}, respectively. The blends show the presence of two C═O and two NH bands; there is no shift in the stretching frequencies with respect to the pure components, which indicates that there is neither an exchange of hydrogen bonds between C_{12} and KemS nor any disruption of hydrogen bonds.

C_{12}/KemE Blends. Figure 5 shows the optical micrographs of C_{12}/KemE blends. The slow-cooled samples containing 2−10% KemE show imperfect spherulites (Figure 5a). The slow-cooled sample containing 15% KemE shows positive spherulites, whereas the sample having 20% KemE shows negative spherulites (parts b and c of Figure 5, respectively). The quenched samples containing 2−15% KemE show spherulitic morphology with very low birefringence. The quenched sample containing 20% KemE does not show any crystal/spherulite under optical microscopy. Both the slow-cooled and quenched blends of C_{12}/KemE show excellent transparency that is comparable to what we obtained in our previous study,[9] from the blends of homologous carbamates.

The slow-cooled samples of KemE and the blends containing 2−10% KemE show imperfect four-leaf-clover patterns in SALS, consistent with the optical microscopy observations. The slow-cooled samples containing 15% and 20% KemE and the quenched samples containing 2−15% KemE show regular four leaf clover patterns in SALS. The SALS patterns for the quenched samples of C_{12} and their blends are presented in Figure 6. The H_v scattering patterns were recorded with the same sample−film distance for all these samples. The figure shows that the four-leaf-clover pattern becomes larger with increasing incorporation of KemE in the blends, indicating a decrease in the size of the spherulites. Figure 7 shows that the spherulite size decreases with an increase in the concentration of KemE in C_{12}. It should be noted that the spherulite size obtained from the slow-cooled sample of 80/20 blend of C_{12}/C_{16} (where the subscript denotes the number of carbons at the alkyl side chain) in our previous study[9] was 10 μm, which is comparable with the 80/20 blend of C_{12}/KemE in this study. Figure 8 shows a comparison in transparency between the slow-cooled samples of C_{12} (Figure 8a) and its 80/20 blends with PE, KemS, and KemE (Figure 8, parts b, c, and d, respectively). To take these photographs, samples of C_{12} and 80/20 blends of PE, KemS,

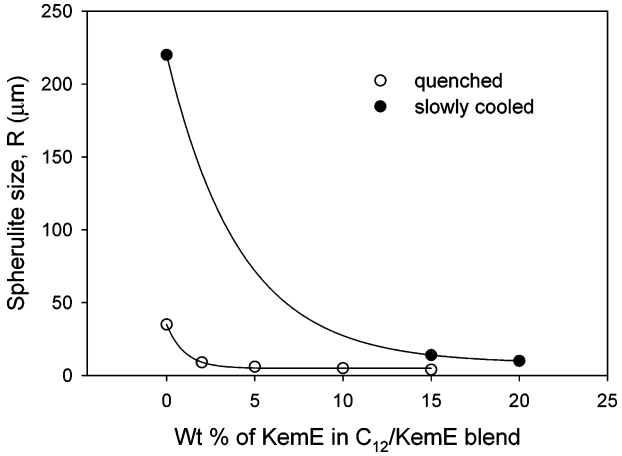

Figure 7. Spherulite size as a function of weight percent of KemE in C_{12}/KemE blends.

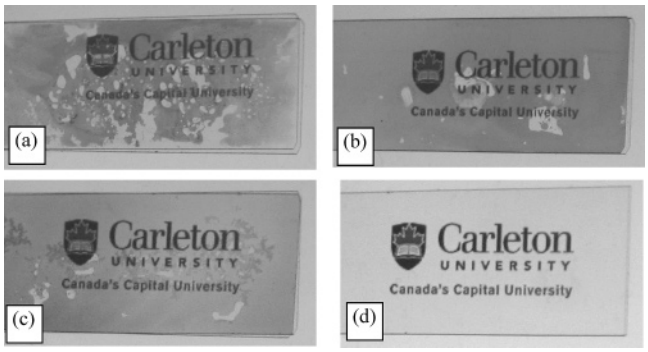

Figure 8. Comparison of the transparency of the various blends: (a) slow-cooled C_{12} and 80/20 blends with (b) PE, (c) KemS, and (d) KemE.

and KemE were melted individually between two microscope slides and were slow-cooled. The graphic on a transparency slide containing the logo and the text was covered with the microscope slide and was projected on a screen. The figure clearly shows the significant improvement in transparency in the 80/20 blend of C_{12}/KemE.

The melting points of both C_{12} and KemE are 74 °C. Similar to C_{12}/PE and C_{12}/KemS blends, C_{12}/KemE blends extert a mutual diluent effect, resulting in a depression of melting points of both C_{12} and KemE. For example, in the DSC thermogram of the slow-cooled blend containing 20% KemE, the melting peak of C_{12} appears at 71 °C and the melting peak of KemE appears as a shoulder at 68 °C.

In contrast to the X-ray diffractograms of C_{12}/PE and C_{12}/KemS blends, the X-ray diffractograms of C_{12}/KemE blends, slow-cooled or quenched, indicate significant changes in the crystal structure of C_{12}. Figure 9 shows that increasing incorporation of KemE in the blend results in a reduction of number of peaks as well as their broadening. The sharp peak of C_{12} at $2\theta = 22.8°$ ($d = 3.9$ Å), which corresponds to the plane of hydrogen bonding,[9] becomes a broad hump in the 80/20 blend of C_{12}/KemE, indicating a significant decrease in crystallinity in the sample. Figure 10 shows the crystallite size and the full width at half-maximum (fwhm) at $d = 3.9$ Å, as a function of blend composition. There is an increase in the fwhm and a decrease in the crystallite size as the amount of KemE increases in the blend. For 80/20 blends of C_{12}/KemE, the fwhm increases from 0.37 to 1.95 rad on the 2θ scale and the crystallite size decreases from 230 to 60 Å.

The IR spectra of C_{12}/KemE blends show some noticeable changes. The C═O stretching frequency of KemE is 1636 cm^{-1}.

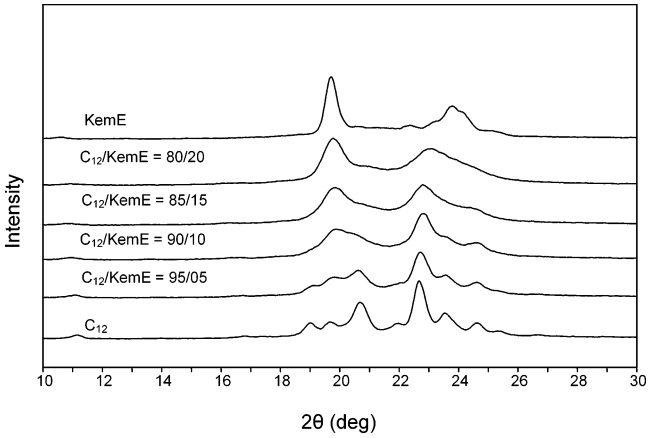

Figure 9. X-ray diffractograms of the binary blends of C_{12}/KemE along with those of C_{12} and KemE.

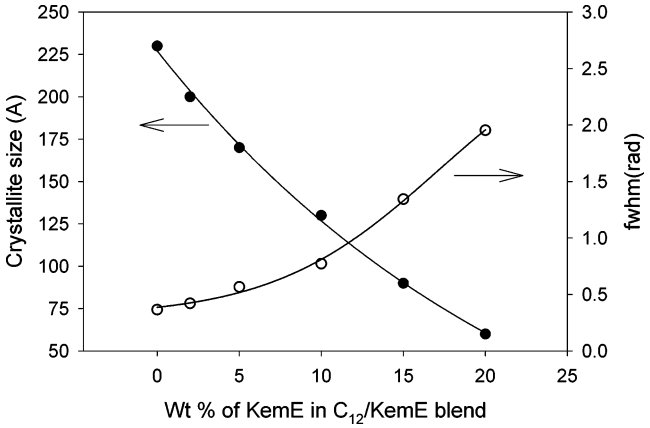

Figure 10. The crystallite size and the full width at half-maximum corresponding to the reflection at 22.8° as a function of C_{12}/KemE blend composition.

TABLE 1: C═O and NH Frequency of C_{12}/KemE Blends

wt % of KemE	υC═O (cm^{-1})	υNH (cm^{-1})	wt % of KemE	υC═O (cm^{-1})	υNH (cm^{-1})
0	1686	3337	40	1686, 1647	3330
5	1686	3337	50	1686, 1644	3330
10	1686, 1659	3336	60	1686, 1641	3330
15	1686, 1658	3335	80	1686, 1638	3330
20	1686, 1657	3335	100	1636	3330

The blends show two carbonyl bands, one at 1686 and another at 1658 cm^{-1}. The intensity of the carbonyl band at 1658 cm^{-1} increases as the amount of KemE increases in the blend. The carbonyl band at 1658 cm^{-1} indicates the possibility that there might be some exchange of hydrogen bonds between C_{12} and KemE. To further explore this possibility, we extended the series by preparing blends containing 20, 40, 50, 60, and 80% KemE. Table 1 shows the C═O and NH stretching frequencies of all the blends. It is seen that the NH bands of C_{12} and KemE are very close; therefore, they merge into one band in the blend. This table, as well as Figure 11, shows that there is a gradual shift of C═O stretching frequency of KemE as the amount of C_{12} increases in the blend. It seems that at higher concentration of C_{12} in the blend, some of the C_{12} molecules form H-bonds with KemE, resulting in a shift of C═O stretching frequency of KemE. When KemE is the major component, there is not much interchange of H-bonds between C_{12} and KemE, since KemE forms stronger H-bonds among themselves. If there is an interchange of hydrogen bonds between C_{12} and KemE, then the insertion of KemE in C_{12} network will provide a misfit in the crystal lattice of C_{12}, which explains the decrease in

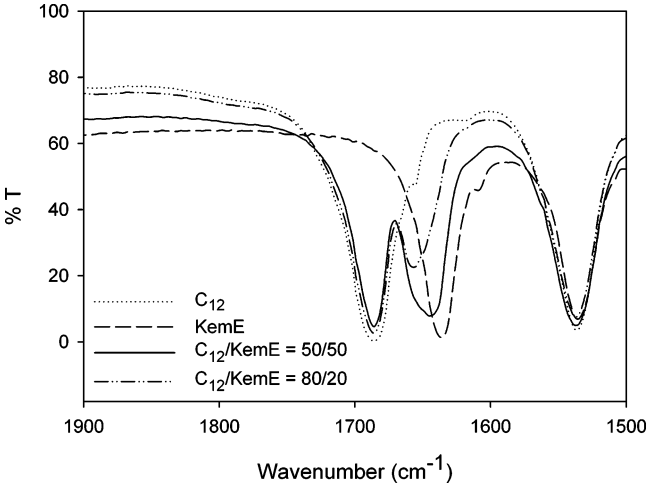

Figure 11. FTIR spectra of C_{12}, KemE, and their blends.

crystallinity in the blends evident from their X-ray diffraction patterns. This decrease in crystallinity has contributed significantly to improve the transparency of the samples. In fact, there are examples in the literature[14] where the nucleating ability of a substance was found to be greater if it can provide a small crystallographic misfit.

The question arises as to why the same change is not happening in the case of KemS. It might be that it is the molecular structure of KemE that is favoring the exchange of H-bonds. The hydrogen-bondable group forms the headgroup in KemS (Figure 1). On the other hand, in both C_{12} and KemE, the hydrogen-bondable group is positioned between the long alkyl chains. This might facilitate the alignment of the C_{12} and KemE and therefore an easy exchange of H-bonds. This also explains the changes we observed in the case of the blends of homologous carbamates. Their structural similarities and similar strength of H-bonds favor the exchange of H-bonds. Although it does not affect the extent of hydrogen bonding, as is evident from the IR, it does affect the packing of alkyl chains, which results in a decrease in crystallinity and heat of fusion and a significant improvement in transparency.

Conclusions

The spherulite size of the carbamate is unaffected up to 5 wt % of PE and KemS in the blend. Further increase in the weight percent of PE or KemS in the blend reduces the spherulite size of the carbamate. However, phase separation occurs with all compositions of KemS in the blend. PE was found to be more effective in reducing the spherulite size of the carbamates. Neither PE nor KemS affects the type or extent of hydrogen bonding of the carbamate. The crystal structure of the carbamate is not affected by the addition of PE or KemS, and the transparency of the sample does not improve significantly as compared to that of pure carbamate. Thus, the reduction in the spherulite size of C_{12} in these blends is due to the small crystals of PE or KemS acting as nucleating agents; this did not improve the transparency, due to phase separation.

On the other hand, significant improvement of the transparency was achieved when the carbamate was blended with KemE. Blending reduces the crystallite and spherulite size, heat of fusion, and crystallinity. The sign of birefringence of the spherulites changes from positive to negative as the weight percent of KemE increases in the blend. FTIR spectra indicate an exchange of hydrogen bonds between the carbamate and KemE. Insertion of KemE in the hydrogen-bonded network of the carbamate causes a misfit in the crystal lattice of the carbamate, which reduces the crystallinity of the carbamate. The change in packing of the alkyl chains of the carbamate is reflected by the broadening of the peak at $d = 3.9$ Å in the X-ray diffractogram, which corresponds to the plane of hydrogen bonding, i.e., the distance between two alkyl chains.

Although there are several theories regarding the heterogeneous nucleation,[14−20] it is still somewhat a mystery as to the mechanism of the nucleating agents.[21] As a result, searching for effective nucleating agents is more or less an empirical process. Although the heterogeneous nucleation of C_{12} by PE and KemS results in the reduction of spherulite/crystal size, they cannot provide as much transparency as has been achieved by KemE or by blending two homologous sets of carbamates with one another. In both of the latter cases a misfit of crystal lattice occurs, due to the intercalation of the components and the poor packing of the alkyl chains. Clearly, H-bonding plays an important role in controlling the morphology of these self-assembling carbamate systems. The findings of this study can help in the design of an effective nucleating agent to control the morphology of self-assembling systems.

Acknowledgment. This work was supported by the Natural Sciences and Engineering Research Council of Canada (NSERC) and Xerox Research Centre of Canada. M.M. was partly supported by the Ontario Graduate Scholarship for Science and Technology (OGSST).

References and Notes

(1) Steichele, K. Belg. Patent 882,922, 1980; *Chem. Abstr. 94*, 66768d.
(2) Saka, K.; Noda, K. Jpn. Kokai Tokkyo Koho JP 62 179 584, 1987; *Chem. Abstr. 108*, 39820r.
(3) Tanaka, K.; Kano, Y.; Yoshida, K. Jpn. Kokai Tokkyo Koho JP 63 248 894 1988; *Chem. Abstr. 110*, 79137w.
(4) Kinoshita, H.; Sekiya, M.; Mishima, M. Eur. Pat. EP 274 756, 1988; *Chem. Abstr. 109*, 233979k.
(5) Jpn. Kokai Tokkyo Koho JP 58 201 758, 1983; *Chem. Abstr. 100*, 174289z.
(6) Tanaka, T.; Yoshitomi, T.; Hanada, Y.; Ohashi, M.; Takeda, Y. Jpn. Kokai Tokkyo Koho JP 6 290 289; *Chem. Abstr. 107*, 20896b.
(7) Goodbrand, B.; Boils, D.; Sundararajan, P. R.; Wong, R.; Malhotra, S. U.S. Patent 6,187,082, 2001.
(8) Goodbrand, B.; Boils, D. C.; Sundararajan, P. R.; Wong, R. W. U.S. Patent 6,414,051, 2002
(9) Moniruzzaman, M.; Goodbrand. B.; Sundararajan, P. R. *J. Phys. Chem. B* **2003**, *107*, 8416.
(10) Moniruzzaman, M.; Sundararajan, P. R. *Pure Appl. Chem.* **2004**, *76*, 1353.
(11) Alexander, L. E. *X-ray Diffraction Methods in Polymer Science*; 1st ed.; Wiley-Interscience: New York, 1969; pp 335.
(12) Jabarin, S. A.; Stein, R. S. *J. Phys. Chem.* **1973**, *77*, 399.
(13) Stein, R. S.; Rhodes, M. B. *J. Appl. Phys.* **1960**, *31*, 1873.
(14) Dovbreva, A.; Alonso, M.; Gonzalez, M.; DE Saja, J. A. *J. Appl. Polym. Sci.* **1997**, *63*, 349.
(15) Willems, J. W. *Experimentia* **1967**, *23*, 409.
(16) Mauritz, K. A.; Baer, E.; Hopfinger, A. J. *J. Polym. Sci., Macromol. Rev.* **1978**, *13*, 1.
(17) Binsbergen, F. L. *Polymer* **1970**, *11*, 253.
(18) Binsbergern, F. L. *J. Polym. Sci., Polym. Symp.* **1977**, *59*, 11.
(19) Lotz, B.; Wittmann, J. C.; *J. Polym. Sci., Part B: Polym. Phys.* **1981**, *25*, 1079.
(20) Lotz, B.; Wittmann, J. C. *Macromol. Chem.* **1984**, *185*, 2043.
(21) Mercier, J. P. *Polym. Eng. Sci.* **1990**, *30*, 270.